

# Large presence of carbonic acid in CO<sub>2</sub>-rich aqueous fluids under Earth's mantle conditions

Nore Stolte<sup>1</sup> and Ding Pan<sup>1,2,3,\*</sup>

<sup>1</sup>*Department of Physics, Hong Kong University of Science and Technology, Hong Kong, China*

<sup>2</sup>*Department of Chemistry, Hong Kong University of Science and Technology, Hong Kong, China*

<sup>3</sup>*HKUST Fok Ying Tung Research Institute, Guangzhou, China*

(Dated: July 4, 2019)

## Abstract

The chemistry of carbon in aqueous fluids at extreme pressure and temperature conditions is of great importance to Earth's deep carbon cycle, which substantially affects the carbon budget at Earth's surface and global climate change. At ambient conditions, the concentration of carbonic acid in water is negligible, so aqueous carbonic acid was simply ignored in previous geochemical models. However, by applying extensive ab initio molecular dynamics simulations at pressure and temperature conditions similar to those in Earth's upper mantle, we found that carbonic acid can be the most abundant carbon species in aqueous CO<sub>2</sub> solutions at  $\sim 10$  GPa and 1000 K. The mole percent of carbonic acid in total dissolved carbon species increases with increasing pressure along an isotherm, while its mole percent decreases with increasing temperature along an isobar. In CO<sub>2</sub>-rich solutions, we found significant proton transfer between carbonic acid molecules and bicarbonate ions, which may enhance the conductivity of the solutions. The effects of pH buffering by carbonic acid may play an important role in water-rock interactions in Earth's interior. Our findings suggest that carbonic acid is an important carbon carrier in the deep carbon cycle.

## INTRODUCTION

The global carbon cycle is of great importance to Earth's climate, human's energy consumption, and sustainable development. Although a tremendous number of studies have focused on the carbon cycle in the atmosphere, oceans, and the shallow crust, less is known about the carbon cycle in Earth's deep interior [1], which may host more than 90% of Earth's carbon [2] and also actively exchanges carbon with Earth's near-surface reservoirs through volcanism and subduction [3, 4]. In the deep carbon cycle, fluids containing water as a primary component play a key role in transporting carbon in the deep mantle and back to magmas in volcanoes and eventually to the atmosphere as carbon dioxide ( $\text{CO}_2$ ) [3, 5]. However, many basic questions about carbon-bearing aqueous fluids are poorly known; for example, what are the aqueous carbon species in the deep carbon cycle? A major obstacle to understanding deep carbon transport is the lack of knowledge of carbon reactions in water at the extreme conditions found in Earth's deep interior [6].

Both pressure (P) and temperature (T) increase with increasing depth inside Earth. For example, in the upper mantle, pressure can reach  $\sim 13$  GPa and temperature  $\sim 1700$  K [7]. Most crust and mantle fluids are at vapor-liquid supercritical conditions, and their properties differ fundamentally from those at ambient or near-ambient conditions, which has been shown by many recent studies [8]. For oxidized carbon dissolved in water, many geochemical models assume that  $\text{CO}_2(\text{aq})$  is the major carbon species, e.g., Refs [9–12], but recent studies show that carbon-containing ions,  $\text{HCO}_3^-$  and  $\text{CO}_3^{2-}$ , may be more abundant than  $\text{CO}_2(\text{aq})$  in Earth's mantle [13, 14].

Another possible oxidized carbon species is carbonic acid ( $\text{H}_2\text{CO}_3$ ) [15, 16]. At ambient conditions, dry  $\text{H}_2\text{CO}_3$  is very stable with a half-life as long as 180,000 years [17], whereas in water it decomposes rapidly and its concentration is only about 0.1% of  $\text{CO}_2(\text{aq})$  concentration [6]; thus, in geochemical modeling  $\text{H}_2\text{CO}_3(\text{aq})$  has simply been treated as  $\text{CO}_2(\text{aq})$ , except in a very recent model [18]. At 2.4 GPa and 553 K, Wang et al. found possible spec-

troscopic evidence of  $\text{H}_2\text{CO}_3(\text{aq})$ , suggesting it might be an important species in aqueous  $\text{CO}_2$  solutions under extreme conditions [19], whereas Abramson et al. commented that the new vibrational band could be also attributed to  $\text{HCO}_3^-$  at high concentration [20]. Note that these experimental P-T conditions can only be found in the shallow or cold mantle areas. It is very challenging to experimentally detect carbon species at *both* high pressures (HP) *and* high temperatures (HT), as found in the deep mantle. In our previous theoretical work, we applied ab initio molecular dynamics simulations to study  $\text{CO}_2$  in water at  $\sim 11$  GPa and 1000 K, and found that about 80% of dissolved carbon is  $\text{HCO}_3^-$  and 10~20%  $\text{H}_2\text{CO}_3(\text{aq})$  as a minor product [14]. The solution is very dilute with  $x(\text{CO}_2) = 0.016$ . In fact, carbon-bearing fluids in deep Earth may range from water-rich to  $\text{CO}_2$ -rich [21]. The carbon speciation in  $\text{CO}_2$ -rich aqueous fluids under Earth's mantle conditions is still unknown.

Here, by applying extensive ab initio molecular dynamics (AIMD) simulations, we studied the  $\text{CO}_2$ - $\text{H}_2\text{O}$  mixtures at various concentrations from 3 to 11 GPa and between 1000 and 1400 K, P-T conditions similar to those in subduction zones in Earth's upper mantle. Our total simulation time exceeds 3.8 nanoseconds. We found that at  $\sim 10$  GPa and 1000 K,  $\text{H}_2\text{CO}_3(\text{aq})$  can be the predominant carbon species in the aqueous  $\text{CO}_2$  solutions. With increasing pressure along an isotherm, the mole percent of  $\text{H}_2\text{CO}_3(\text{aq})$  in total dissolved carbon species increases, while with increasing temperature along an isobar, its mole percent decreases. We show the possible P-T range where  $\text{H}_2\text{CO}_3(\text{aq})$  may exist. The rich chemistry of  $\text{H}_2\text{CO}_3(\text{aq})$  may play an important role in the dissolution of carbonate minerals in aqueous fluids in deep Earth. Our findings suggest that  $\text{H}_2\text{CO}_3(\text{aq})$  is an important carbon carrier in the deep carbon cycle.

## RESULTS AND DISCUSSION

### Equation of state of CO<sub>2</sub>-H<sub>2</sub>O mixtures

First, we calculated the equation of state (EOS) of CO<sub>2</sub>-H<sub>2</sub>O mixtures given by density functional theory (DFT) with the PBE exchange-correlation functional. In previous studies we used the same level of theory to calculate many properties of water under HP-HT conditions, such as equation of state [22], dielectric constant [23], Raman and IR spectra, and ionic conductivity [24], as well as the reactions of CO<sub>2</sub> and carbonates in HP-HT water [14]. In Table SI, we compare the DFT pressures of CO<sub>2</sub>-H<sub>2</sub>O systems with those obtained by popular geochemical models [10, 11] and classical force-field MD simulations at various CO<sub>2</sub> concentrations. The force field is from Duan and Zhang’s work in 2006 [10]. Since the EOS in Ref. [10] was obtained by fitting the MD simulation data using the force field and the experimental data, it is not surprising the pressures calculated by Duan and Zhang’s EOS in Ref. [10] are in excellent agreement with those calculated by our MD simulations with the same force field. The EOS pressures of Ref. [10] are generally smaller than the results obtained by Zhang and Duan’s EOS [11] in 2009, which was designed for C-O-H fluids in Earth’s mantle. It was recently reported [25] that for CO<sub>2</sub>-H<sub>2</sub>O binary systems, the EOS in Ref. [10] performs better than the one in Ref. [11].

In our simulations, we varied the initial mole fraction of CO<sub>2</sub>(aq), which is defined as  $x(\text{CO}_2) = \frac{n(\text{CO}_2)}{n(\text{CO}_2)+m(\text{H}_2\text{O})}$ , where  $n(\text{CO}_2)$  and  $m(\text{H}_2\text{O})$  are the numbers of CO<sub>2</sub> and water molecules, respectively. When  $x(\text{CO}_2)$  is smaller than 0.1, our DFT pressures are slightly larger than those obtained by the EOS in Ref. [10], while for  $x(\text{CO}_2)$  larger than 0.1, the DFT pressures become smaller. Note that in the simulations using the force field from Ref. [10], no chemical reaction occurs between CO<sub>2</sub> and water, whereas in the ab initio simulations the carbon atoms may be converted from sp to sp<sup>2</sup> hybridization, and vice versa. The newly generated carbon species may have different molecular volumes, which affect the EOS of

the mixtures. Overall, the agreement between our ab initio data and available EOS data is satisfactory, indicating that the PBE functional is not only suitable for water under extreme conditions, but may also be used to study CO<sub>2</sub>-H<sub>2</sub>O mixtures at HP and HT.

### Speciation of CO<sub>2</sub>-H<sub>2</sub>O mixtures

Fig. 1(A) shows the relative concentrations of carbon species as functions of  $x(\text{CO}_2)$  obtained from AIMD simulations at  $\sim 10$  GPa and 1000 K. The mole percents of CO<sub>2</sub>(aq), HCO<sub>3</sub><sup>-</sup>, CO<sub>3</sub><sup>2-</sup>, and H<sub>2</sub>CO<sub>3</sub>(aq) as functions of simulation time are shown in Fig. S1. With increasing  $x(\text{CO}_2)$ , the mole percent of HCO<sub>3</sub><sup>-</sup> in total dissolved carbon species decreases, and more CO<sub>2</sub>(aq) molecules were found in the simulations. The crossover between HCO<sub>3</sub><sup>-</sup> and CO<sub>2</sub>(aq) happens when  $x(\text{CO}_2)$  is about 0.25. We found few carbonate ions, and the mole percent of CO<sub>3</sub><sup>2-</sup> is less than 10% in all the simulations in Fig. 1. Interestingly, when  $x(\text{CO}_2)$  is in the range of 0.14 to 0.31, carbonic acid becomes the predominant carbon species, more abundant than any other carbon-containing molecules or ions. When increasing  $x(\text{CO}_2)$  up to  $\sim 0.20$ , the mole percent of H<sub>2</sub>CO<sub>3</sub>(aq) reaches its maximum ( $\sim 47\%$ ); at higher  $x(\text{CO}_2)$ , the mole percent of H<sub>2</sub>CO<sub>3</sub> slowly decreases. During the decrease, H<sub>2</sub>CO<sub>3</sub>(aq) is always more abundant than HCO<sub>3</sub><sup>-</sup>. After increasing the temperature from 1000 K to 1400 K at  $\sim 10$  GPa, the HCO<sub>3</sub><sup>-</sup>-CO<sub>2</sub> crossover happens at a lower carbon concentration with  $x(\text{CO}_2) = 0.10$  (Fig. 1(B)). At 1400 K, the mole percent of H<sub>2</sub>CO<sub>3</sub>(aq) is about 20% when  $x(\text{CO}_2)$  is between 0.03 and 0.33, and does not have a clear maximum value.

### Molecular geometry of H<sub>2</sub>CO<sub>3</sub>

The carbonic acid molecule has one carbon atom and three oxygen atoms, which form the trigonal planar shape [26, 27]. Two hydrogen atoms, which are each bonded to an oxygen atom, appear not always in the plane of the carbon and oxygen atoms in the MD simulations. Fig. 2 shows the distribution of the two O=C-O-H dihedral angles. The H<sub>2</sub>CO<sub>3</sub>

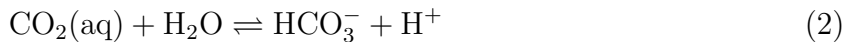
conformer with the lowest free energy is the cis-cis conformer, where the two dihedral angles are both  $0^\circ$ . The conformer with the second lowest free energy is cis-trans, where the two dihedral angles are  $0^\circ$  and  $180^\circ$ . The trans-trans conformer, where the two dihedral angles are both  $180^\circ$ , has much higher free energy than the former two. We calculated the free energy difference between the  $i$ th and  $j$ th conformer by  $\Delta F = -k_B T \ln\left(\frac{P_i}{P_j}\right)$ , where  $k_B$  is the Boltzmann constant and  $P_i$  is the probability of the  $i$ th conformer. The free energies are calculated with respect to the cis-cis conformer. At  $\sim 10$  GPa and 1000 K, the free energy of the cis-trans conformer is 0.14 kcal/mol (0.006 eV), while the trans-trans conformer has the free energy of 1.82 kcal/mol (0.079 eV). When increasing the temperature from 1000 to 1400 K along the isobar of  $\sim 10$  GPa, the free energy of the cis-trans conformer increases to 0.19 kcal/mol (0.008 eV), while the trans-trans one increases to 2.31 kcal/mol (0.100 eV).

In the gas phase at 0 K, the free energies of the cis-trans and trans-trans conformers are 1.6 and 10.1 kcal/mol respectively [26], much higher than the respective free energies in the aqueous solutions studied here. This may be attributed to the dielectric screening of water. The three  $\text{H}_2\text{CO}_3$  conformers have different electrostatic interactions. The two hydrogen atoms with partial positive charges in the trans-trans conformer are closer than in the other two conformers, so the stronger electrostatic repulsive force causes a higher energy in the trans-trans conformer. Because the dielectric screening of water weakens electrostatic interactions, we see the lower free energies for the trans-trans and cis-trans conformers in water than in the gas phase. When increasing T along an isobar, the dielectric constant of water decreases [22], so the screening becomes weaker and the free energies become larger again.

### **Reaction mechanisms of $\text{H}_2\text{CO}_3(\text{aq})$**

In Fig. 3, we analyzed how  $\text{H}_2\text{CO}_3(\text{aq})$  forms and dissociates at  $\sim 10$  GPa and 1000 K. In our AIMD simulations,  $\sim 90\%$  of the  $\text{H}_2\text{CO}_3(\text{aq})$  formation reactions follow a two-step

mechanism [28]: (i) the reaction of  $\text{CO}_2(\text{aq})$  with  $\text{OH}^-$  or water to form  $\text{HCO}_3^-$ ,



and (ii) the protonation of  $\text{HCO}_3^-$  to form  $\text{H}_2\text{CO}_3(\text{aq})$ :



Because the solutions are acidic, it is very rare to see free  $\text{OH}^-$ . In reaction (1), the  $\text{OH}^-$  ion is often associated with the  $\text{H}_3\text{O}^+$  ion generated by the self-ionization of water. If the proton keeps hopping between the  $\text{OH}^-$  and  $\text{H}_3\text{O}^+$  ions, reaction (1) will also go backward and forward frequently. When the proton in  $\text{H}_3\text{O}^+$  transfers away from the ion pair along a hydrogen-bond wire via the Grotthuss mechanism [29], the chemical equilibrium of reaction (1) shifts to the right. Similarly, in reaction (2) where the  $\text{CO}_2$  molecule reacts with a water molecule, if the released proton is accepted by a third species and cannot transfer back, the generated  $\text{HCO}_3^-$  will not often change back to  $\text{CO}_2(\text{aq})$ .

In reaction (3), the  $\text{HCO}_3^-$  ion accepts one proton to become  $\text{H}_2\text{CO}_3(\text{aq})$ . Fig. 3(A) shows that when the carbon concentration is low, most of the protons are from  $\text{H}_3\text{O}^+$ , whereas with increasing  $x(\text{CO}_2)$ , more and more protons come from  $\text{H}_2\text{CO}_3(\text{aq})$ , indicating that protons can transfer between  $\text{HCO}_3^-$  and  $\text{H}_2\text{CO}_3(\text{aq})$  in  $\text{CO}_2$ -rich solutions (see Fig. 4). We even found  $\text{H}_3\text{CO}_3^+$  as an intermediate proton donor with lifetime less than 0.15 ps. In fact, about 10% of  $\text{H}_2\text{CO}_3(\text{aq})$  is generated from the dissociation of  $\text{H}_3\text{CO}_3^+$ :



The  $\text{sp}^2$  carbon species such as  $\text{H}_2\text{CO}_3$ ,  $\text{HCO}_3^-$ , and  $\text{H}_3\text{CO}_3^+$  may form a network to conduct protons in water. It was expected that the ionic conductivity of  $\text{CO}_2$ - $\text{H}_2\text{O}$  mixtures decreases significantly with increasing  $x(\text{CO}_2)$ , if only the self-ionization of water contributes to ionic conduction [8]. This expectation may not be valid, as the generated  $\text{sp}^2$  carbon species can enhance the ionic conductivity.

At  $\sim 10$  GPa and 1000 K, about 90% of  $\text{H}_2\text{CO}_3(\text{aq})$  dissociates to become  $\text{HCO}_3^-$  via backward reaction (3). The lifetime of  $\text{H}_2\text{CO}_3(\text{aq})$  is typically less than 1 ps (see Fig. S4). When the solutions are dilute, most of protons transfer to water molecules to form  $\text{H}_3\text{O}^+$ , whereas with increasing  $x(\text{CO}_2)$ , the role of  $\text{HCO}_3^-$  or  $\text{H}_2\text{CO}_3(\text{aq})$  as proton acceptors becomes more important, as shown in Fig. 3(B). Interestingly, only 1~3% of  $\text{HCO}_3^-$  further decompose into  $\text{CO}_2(\text{aq})$  (see Fig. S5). We found two decomposition pathways: backward reaction (1) and (2). Decomposition via backward reaction (1) is more likely to happen when  $x(\text{CO}_2)$  is low. With increasing  $x(\text{CO}_2)$ , decomposition via backward reaction (2) becomes more frequent. In backward reaction (1), if the  $\text{OH}^-$  ion remains in the first solvation shell of  $\text{CO}_2$ , the  $\text{O}_2\text{C-OH}$  bond often keeps breaking and forming unless the  $\text{OH}^-$  ion accepts a proton and becomes a  $\text{H}_2\text{O}$  molecule. Averagely,  $\text{CO}_2(\text{aq})$  generated through backward reaction (2) has a longer lifetime than that from backward reaction (1). About 10% of  $\text{H}_2\text{CO}_3(\text{aq})$  does not dissociate or decompose, but receives protons to become the intermediate  $\text{H}_3\text{CO}_3^+$  through backward reaction (4). In the gas phase, the decomposition of  $\text{H}_2\text{CO}_3$  occurs via the concerted mechanism that involves the dehydroxylation of one  $\text{OH}^-$  group and the deprotonation of the other  $\text{OH}^-$  group simultaneously [17, 30]. Here, we found only the stepwise process through backward reactions (3), and (2) or (1). Galib and Hanna studied the decomposition mechanism of  $\text{H}_2\text{CO}_3(\text{aq})$  using water clusters with varied sizes at ambient conditions, and found that the hydrogen bonding environment around the  $\text{H}_3\text{O}^+$  ion as found in bulk water leads to stepwise decomposition [31], which indicates that at the supercritical conditions studied here there are still strong water-ion bonding interactions.

The reaction mechanisms of  $\text{H}_2\text{CO}_3(\text{aq})$  formation and dissociation help us understand why  $\text{H}_2\text{CO}_3(\text{aq})$  can be the predominant carbon species in supercritical water at  $\sim 10$  GPa and 1000 K. When the  $\text{CO}_2\text{-H}_2\text{O}$  solution is dilute, most  $\text{CO}_2$  reacts and becomes  $\text{HCO}_3^-$  via reaction (1) or (2) [14]. With increasing  $x(\text{CO}_2)$ , the solution becomes more acidic and  $\text{HCO}_3^-$  stays closer to  $\text{H}_3\text{O}^+$ , so reaction (3) is more likely to happen. Thus, when increasing  $x(\text{CO}_2)$  up to  $\sim 0.20$ , the concentration of  $\text{H}_2\text{CO}_3(\text{aq})$  increases to its maximum.



However, when further increasing  $x(\text{CO}_2)$ , a significant amount of  $\text{CO}_2(\text{aq})$  does not react and the mole percent of  $\text{HCO}_3^-$  in total dissolved carbon species keeps decreasing. As a result, the mole percent of  $\text{H}_2\text{CO}_3(\text{aq})$  also decreases. When  $x(\text{CO}_2) > 0.14$ ,  $\text{H}_2\text{CO}_3(\text{aq})$  is more abundant than  $\text{HCO}_3^-$ , indicating that  $\text{H}_2\text{CO}_3(\text{aq})$  is energetically favored over  $\text{HCO}_3^-$  in  $\text{CO}_2$ -rich solutions under extreme conditions.

**P-T range of  $\text{H}_2\text{CO}_3(\text{aq})$**

When increasing the temperature from 1000 K to 1400 K at  $\sim 10$  GPa, the mole percent of  $\text{H}_2\text{CO}_3(\text{aq})$  becomes smaller. The concentration of  $\text{CO}_2(\text{aq})$  at thermal equilibrium at 1400 K is higher than that at 1000 K when the initial  $\text{CO}_2$  concentration is the same. As a result, the  $\text{H}_2\text{CO}_3$  formation reactions are less likely to happen. Big molecules or ions tend to decompose at high temperatures, so at 1400 K, 9~10% of  $\text{HCO}_3^-$  decomposes into  $\text{CO}_2(\text{aq})$ , almost one order of magnitude more than that at 1000 K.

Not only temperature but also pressure affects the presence of  $\text{H}_2\text{CO}_3(\text{aq})$ . We lowered the pressure from  $\sim 10$  GPa to  $\sim 8.0$  GPa,  $\sim 6.1$  GPa, and  $\sim 3.8$  GPa in the AIMD simulations at 1000 K and  $x(\text{CO}_2) = 0.016$  (see Fig. 1(C)). Because the solutions are dilute,  $\text{H}_2\text{CO}_3(\text{aq})$  is not the predominant carbon species, but we can estimate the formation of  $\text{H}_2\text{CO}_3(\text{aq})$  with increasing  $x(\text{CO}_2)$  based on the reaction mechanisms discussed above. At  $\sim 8.0$  GPa, most of the  $\text{CO}_2$  molecules still convert into  $\text{HCO}_3^-$ , but the concentration of  $\text{HCO}_3^-$  is lower than that at  $\sim 10$  GPa; thus, with increasing  $x(\text{CO}_2)$ , we also expect to have a significant amount of  $\text{H}_2\text{CO}_3(\text{aq})$ , despite a lower concentration than that at  $\sim 10$  GPa. Fig. 1(C) shows that when the pressure is lower than  $\sim 6.3$  GPa,  $\text{CO}_2(\text{aq})$  becomes predominant. Because  $\text{CO}_2(\text{aq})$  reacts slowly at low pressures, the transition pressure of  $\sim 6.3$  GPa should be an upper limit. Generally, with decreasing pressure at 1000 K, the mole percent of  $\text{H}_2\text{CO}_3(\text{aq})$  decreases.

In Fig. 5, we show the possible P-T range for  $\text{H}_2\text{CO}_3(\text{aq})$  as a significant solute in

water based on our AIMD simulations and experimental findings. With increasing P along an isotherm, the concentration of  $\text{H}_2\text{CO}_3(\text{aq})$  increases, while with increasing T along an isobar, less  $\text{H}_2\text{CO}_3(\text{aq})$  forms. There can be a significant amount of  $\text{H}_2\text{CO}_3(\text{aq})$  at  $P \sim 10$  GPa and  $T \leq 1400$  K. Wang et al. showed possible spectroscopic evidence of  $\text{H}_2\text{CO}_3(\text{aq})$  at 2.4 GPa and 553 K in a mixture of  $\text{CO}_2$  and  $\text{H}_2\text{O}$  [19]. For aqueous  $\text{CO}_2$  solutions, Abramson et al. found that with increasing P from 4.1 GPa to 6.2 GPa at 523 K, the Raman signal of  $\text{CO}_2(\text{aq})$  gradually disappears and a new peak at  $\sim 1040 \text{ cm}^{-1}$  might be attributed to high concentration  $\text{HCO}_3^-$  or  $\text{H}_2\text{CO}_3(\text{aq})$  [20]. No evidence for the formation of  $\text{H}_2\text{CO}_3(\text{aq})$  below 2.4 GPa is reported experimentally, so in Fig. 5 we use 2.4 GPa and 523 K as the P-T boundary of  $\text{H}_2\text{CO}_3(\text{aq})$ . In Fig. 5, we also show the P-T conditions of water in Earth's upper mantle [32] and subducting slab surfaces [33], which largely overlap with the P-T range of the formation of  $\text{H}_2\text{CO}_3(\text{aq})$ . This indicates that there can be a significant amount of  $\text{H}_2\text{CO}_3(\text{aq})$  in aqueous geofluids in subduction zones in the upper mantle. Dissolved  $\text{CO}_2$  in aqueous geofluids may be gradually converted into  $\text{H}_2\text{CO}_3(\text{aq})$  and  $\text{HCO}_3^-/\text{CO}_3^{2-}$  with increasing depth. The  $\text{sp}^2$ -carbon-bearing fluids may also be brought back to Earth's surface by volcanism and the  $\text{CO}_2$  degassing would occur in shallow areas.

In the DFT calculations, we used the semilocal exchange-correlation functional PBE [34]. It has been reported that generalized gradient approximations (GGAs) may not be able to describe doubly charged anions in water accurately at ambient conditions [35]. However, PBE performs better at HP-HT conditions than at ambient conditions, as shown in many of our previous studies [14, 22–24]. Our previous finding that  $\text{CO}_2(\text{aq})$  is absent at  $\sim 11$  GPa and 1000 K [14] was further extended to lower pressures and temperatures by experiment [20], indicating that our computational method is capable to predict the properties of aqueous carbon solutions under extreme conditions. To validate our results, we compared the PBE simulations with the simulations using the hybrid functional PBE0 [14, 36], which often gives results in better agreement with experimental ones due to the smaller charge delocalization error [37]. When we dissolved  $\text{CO}_2$  in water ( $x(\text{CO}_2) = 0.016$ ) at  $\sim 11$  GPa

and 1000 K , we found that in both PBE and PBE0 simulations,  $\text{HCO}_3^-$  is the predominant carbon species and its mole percents are very similar: 79.8% vs. 75.0% [14]. PBE0 predicts even more  $\text{H}_2\text{CO}_3(\text{aq})$  than PBE. Thus, our finding that  $\text{H}_2\text{CO}_3(\text{aq})$  can be the most abundant carbon species under extreme conditions would not be affected by the PBE error.

In addition, van der Waals interactions are not well captured by the PBE and PBE0 functionals. However, previous studies showed that PBE and van der Waals functionals give closer results at high pressure than at ambient pressure for the equilibrium volume and dielectric constant of ice [38], indicating that for water and ice under pressure, the dispersion interactions are not so important as those at ambient conditions. Besides, the breaking and forming of covalent bonds are little affected by weak van der Waals interactions, so the lack of dispersion interactions should not change our main results here.

The chemical reactions involving  $\text{H}_2\text{CO}_3(\text{aq})$  greatly affect the acidity of aqueous carbon solutions, which may have an important impact on water-rock interactions in deep Earth [39]. It has been estimated that about half of carbon in subducting slabs or even more is brought back to Earth's surface [4]. The previous geochemical studies on the devolatilization in subduction zones considered only  $\text{CO}_2(\text{aq})$  as the major carbon species in water [3]. If so, the amounts of carbon removed from subducting slabs are too small to account for the large volumes of carbon found in magmas [3]. It was recently reported that significant quantities of carbonate minerals are dissolved by the infiltrating fluids, and are brought back to magmas, which may potentially balance  $\text{CO}_2$  emissions from volcanoes [40]. However, the chemical mechanism of this dissolution process is not yet known. At HP-HT conditions, the solubilities of carbonate minerals in pure water increase, but are still not very large [13, 22]. If we consider only molecular  $\text{CO}_2$  in the solutions, the solubilities should become even lower [6]. Our current work suggests that the effects of pH buffering by  $\text{H}_2\text{CO}_3(\text{aq})$  may play an important role in enhancing the dissolution of carbonate minerals [39].

## CONCLUSION

In conclusion, we conducted ab initio molecular dynamics simulations to study dissolved  $\text{CO}_2$  in both water-rich and  $\text{CO}_2$ -rich aqueous solutions from 3 to 11 GPa and at 1000 and 1400 K, P-T conditions similar to those found in subduction zones in Earth’s upper mantle. We found that  $\text{H}_2\text{CO}_3(\text{aq})$ , whose concentration is negligible in water at ambient conditions, is the most abundant carbon species in the aqueous  $\text{CO}_2$  solutions at  $\sim 10$  GPa and 1000 K, when the initial mole fraction of  $\text{CO}_2(\text{aq})$  is between 0.14 and 0.31. With increasing pressure along an isotherm, the mole percent of  $\text{H}_2\text{CO}_3(\text{aq})$  in total dissolved carbons species increases, while with increasing temperature along an isobar, its mole percent decreases. Contrary to popular geochemical models assuming carbon mainly exists in the form of molecular  $\text{CO}_2$  in aqueous geofluids, our study suggests that big carbon-containing molecules like  $\text{H}_2\text{CO}_3(\text{aq})$  cannot be ignored under deep Earth conditions. We found significant proton transfer between  $\text{H}_2\text{CO}_3(\text{aq})$  and  $\text{HCO}_3^-$  in  $\text{CO}_2$ -rich solutions, which may enhance the ionic conductivity of the fluids. The rich chemistry of  $\text{H}_2\text{CO}_3(\text{aq})$  may substantially affect water-rock interactions in deep Earth. For example, the effects of pH buffering by  $\text{H}_2\text{CO}_3(\text{aq})$  may play an important role in enhancing the dissolution of carbonate minerals. Our findings suggest that  $\text{H}_2\text{CO}_3(\text{aq})$  is an important carbon carrier in the deep carbon cycle. Not only inside Earth, it may also largely exist in other water-rich planets [41].

## METHODS

### Ab initio molecular dynamics (AIMD)

AIMD simulations were carried out with the Qbox code (version 1.63.8, <http://qboxcode.org/>) [42] in the Born-Oppenheimer approximation. We used plane wave basis sets, the PBE exchange-correlation functional [34], and norm-conserving pseudopotentials with a kinetic energy cutoff of 85 Ry (Pseudopotential Table, <http://fpmd.ucdavis.edu/potentials>) [43, 44].

In the pressure calculations, the cutoff was increased to 145 Ry. We sampled the Brillouin zone of the simulation box at the  $\Gamma$  point only. We used deuterium instead of hydrogen to have a larger time step (0.24 fs) for computational convenience. The temperature was controlled by the Bussi-Donadio-Parrinello thermostat ( $\tau = 24.2$  fs) [45]. The numbers of CO<sub>2</sub> and water molecules in simulation boxes are listed in Table SI. In MD simulations, the equilibration time is 20 ps. Each production run is between 180 and 580 ps long, as shown in Fig. S1-S3.

We used the atomic trajectories obtained from AIMD simulations to determine the chemical form of carbon species. To determine whether a carbon atom is sp or sp<sup>2</sup> hybridized, we sorted the three smallest C-O distances near each carbon atom. If the difference between the second and third C-O distances is more than 0.4 Å, the species was defined as CO<sub>2</sub>; otherwise, it was considered as a CO<sub>3</sub><sup>2-</sup> anion. For each hydrogen atom near carbon species, we looked for the closest oxygen atom to form the O-H bond. The bicarbonate ion and carbonic acid have one and two O-H bonds, respectively.

### **Classical molecular dynamics**

Classical MD simulations were performed using simulation boxes containing 320~512 molecules. We used the Gromacs package version 5.1.2 [46]. The time step is 1 fs. The force fields for CO<sub>2</sub> and water are from Ref. [10]. The temperature was maintained by the Bussi-Donadio-Parrinello thermostat ( $\tau = 0.1$  ps). Electrostatic interactions were calculated using the fast smooth particle-mesh Ewald method with a grid spacing of 1 Å and cubic interpolation. A cutoff radius of 10 Å was used for van der Waals interactions. Production runs are ~2 ns after 1 ns equilibration.

## ACKNOWLEDGEMENTS

We thank Giulia Galli and Viktor Rozsa for their helpful discussions. N.S. acknowledges the Hong Kong PhD Fellowship Scheme. D.P. acknowledges support from the Croucher Foundation through the Croucher Innovation Award, Hong Kong Research Grants Council (Projects ECS-26305017, GRF-16307618), National Natural Science Foundation of China (Project 11774072), and the Alfred P. Sloan Foundation through the Deep Carbon Observatory.

## CONTRIBUTIONS

D.P. designed the research. N.S. performed the ab initio and classical simulations. All authors contributed to the analysis and discussion of the data and the writing of the manuscript.

---

\* dingpan@ust.hk

- [1] Hazen RM, Schiffries CM (2013) Why deep carbon? *Rev. Mineral. Geochem.* 75(1):1–6.
- [2] Falkowski P, et al. (2000) The global carbon cycle: A test of our knowledge of Earth as a system. *Science* 290:291–296.
- [3] Manning CE (2014) A piece of the deep carbon puzzle. *Nat. Geosci.* 7:333–334.
- [4] Kelemen PB, Manning CE (2015) Reevaluating carbon fluxes in subduction zones, what goes down, mostly comes up. *Proc. Natl. Acad. Sci. U.S.A.* 112(30):E3997–E4006.
- [5] Manning CE (2004) The chemistry of subduction-zone fluids. *Earth Planet. Sci. Lett.* 223(1-2):1–16.
- [6] Manning CE, Shock EL, Sverjensky DA (2013) The chemistry of carbon in aqueous fluids at crustal and upper-mantle conditions: experimental and theoretical constraints. *Rev. Mineral.*

- Geochem.* 75(1):109–148.
- [7] Frost DJ (2008) The upper mantle and transition zone. *Elements* 4:171–176.
- [8] Manning CE (2018) Fluids of the lower crust: Deep is different. *Annu. Rev. Earth Planet. Sci.* 46:67–97.
- [9] Mäder UK, Berman RG (1991) An equation of state for carbon dioxide to high pressure and temperature. *Am. Mineral.* 76:1547–1559.
- [10] Duan Z, Zhang Z (2006) Equation of state of the H<sub>2</sub>O, CO<sub>2</sub>, and H<sub>2</sub>O-CO<sub>2</sub> systems up to 10 GPa and 2573.15 K: Molecular dynamics simulations with ab initio potential surface. *Geochim. Cosmochim. Acta* 70:2311–2324.
- [11] Zhang C, Duan Z (2009) A model for C-O-H fluid in the Earth’s mantle. *Geochim. Cosmochim. Acta* 73:2089–2102.
- [12] Holland TJB, Powell R (2011) An improved and extended internally consistent thermodynamic dataset for phases of petrological interest, involving a new equation of state for solids. *J. Metamorphic Geol.* 29:333–383.
- [13] Facq S, Daniel I, Montagnac G, Cardon H, Sverjensky DA (2014) In situ Raman study and thermodynamic model of aqueous carbonate speciation in equilibrium with aragonite under subduction zone conditions. *Geochim. Cosmochim. Acta* 132:375–390.
- [14] Pan D, Galli G (2016) The fate of carbon dioxide in water-rich fluids under extreme conditions. *Sci. Adv.* 2(10):e1601278.
- [15] Adamczyk K, Prémont-Schwarz M, Pines D, Pines E, Nibbering ETJ (2009) Real-time observation of carbonic acid formation in aqueous solution. *Science* 326(5960):1690–1694.
- [16] Loerting T, Bernard J (2010) Aqueous carbonic acid (H<sub>2</sub>CO<sub>3</sub>). *ChemPhysChem* 11(11):2305–2309.
- [17] Loerting T, et al. (2000) On the surprising kinetic stability of carbonic acid (H<sub>2</sub>CO<sub>3</sub>). *Angew. Chem. Int. Ed.* 39(5):891–894.

- [18] Huang F, Sverjensky DA (2019) Extended deep earth water model for predicting major element mantle metasomatism. *Geochim. Cosmochim. Acta* 254:192–230.
- [19] Wang H, Zeuschner J, Eremets M, Troyan I, Willams J (2016) Stable solid and aqueous  $\text{H}_2\text{CO}_3$  from  $\text{CO}_2$  and  $\text{H}_2\text{O}$  at high pressure and high temperature. *Sci. Rep.* 6:19902.
- [20] Abramson EH, Bollengier O, Brown JM (2017) The water-carbon dioxide miscibility surface to  $450^\circ\text{C}$  and 7 GPa. *Am. J. Sci.* 317:967–989.
- [21] Andersen T, Neumann ER (2001) Fluid inclusions in mantle xenoliths. *Lithos* 55(1-4):301–320.
- [22] Pan D, Spanu L, Harrison B, Sverjensky DA, Galli G (2013) Dielectric properties of water under extreme conditions and transport of carbonates in the deep Earth. *Proc. Natl. Acad. Sci. U.S.A.* 110(17):6646–6650.
- [23] Pan D, Wan Q, Galli G (2014) The refractive index and electronic gap of water and ice increase with increasing pressure. *Nat. Commun.* 5:3919.
- [24] Rozsa V, Pan D, Giberti F, Galli G (2018) Ab initio spectroscopy and ionic conductivity of water under Earth mantle conditions. *Proc. Natl. Acad. Sci. U.S.A.* 115(27):6952–6957.
- [25] Zhang Z, Zhang C, Geng M (2016) Equations of state for aqueous solutions under mantle conditions. *Sci. China Earth Sci.* 59(6):1095–1106.
- [26] Reisenauer HP, Wagner JP, Schreiner PR (2014) Gas-phase preparation of carbonic acid and its monomethyl ester. *Angew. Chem. Int. Ed.* 53(14):11766–11771.
- [27] Bucher G, Sander W (2014) Clarifying the structure of carbonic acid. *Science* 346(6209):544–545.
- [28] Stirling A, Pápai I (2010)  $\text{H}_2\text{CO}_3$  forms via  $\text{HCO}_3^-$  in water. *J. Phys. Chem. B* 114:16854–16859.
- [29] Marx D (2006) Proton transfer 200 years after von Grotthuss: Insights from ab initio simulations. *ChemPhysChem* 7:1848–1870.
- [30] Kumar PP, Kalinichev AG, Kirkpatrick RJ (2007) Dissociation of carbonic acid: Gas phase energetics and mechanism from ab initio metadynamics simulations. *J. Chem. Phys.* 126:204315.



- [31] Galib M, Hanna G (2014) The role of hydrogen bonding in the decomposition of  $\text{H}_2\text{CO}_3$  in water: Mechanistic insights from ab initio metadynamics studies of aqueous clusters. *J. Phys. Chem. B* 118:5983–5993.
- [32] Thompson AB (1992) Water in the Earth’s upper mantle. *Nature* 358(6384):295–302.
- [33] Syracuse EM, van Keken PE, Abers GA (2010) The global range of subduction zone thermal models. *Phys. Earth Planet. Inter.* 183:73–90.
- [34] Perdew JP, Burke K, Ernzerhof M (1996) Generalized gradient approximation made simple. *Phys. Rev. Lett.* 77(18):3865–3868.
- [35] Wan Q, Spanu L, Gygi F, Galli G (2014) Electronic structure of aqueous sulfuric acid from first-principles simulations with hybrid functionals. *J. Phys. Chem. Lett.* 5(15):2562–2567.
- [36] Adamo C, Barone V (1999) Toward reliable density functional methods without adjustable parameters: The PBE0 model. *J. Chem. Phys.* 110(13):6158–6170.
- [37] Cohen AJ, Mori-Sánchez P, Yang W (2008) Insights into current limitations of density functional theory. *Science* 321(5890):792–794.
- [38] Murray ÉD, Galli G (2012) Dispersion interactions and vibrational effects in ice as a function of pressure: A first principles study. *Phys. Rev. Lett.* 108(10):105502.
- [39] Manning CE (2013) Thermodynamic modeling of fluid-rock interaction at mid-crustal to upper-mantle conditions. *Rev. Mineral. Geochem.* 76(1):135–164.
- [40] Ague JJ, Nicolescu S (2014) Carbon dioxide released from subduction zones by fluid-mediated reactions. *Nat. Geosci.* 7:355–360.
- [41] Marounina N, Rogers LA (2019) Internal structure and  $\text{CO}_2$  reservoirs of habitable water-worlds. Preprint at <https://arxiv.org/abs/1904.10458>.
- [42] Gygi F (2008) Architecture of Qbox: A scalable first-principles molecular dynamics code. *IBM J. Res. & Dev.* 52(1/2):137–144.
- [43] Hamann DR, Schlüter M, Chiang C (1979) Norm-conserving pseudopotentials. *Phys. Rev. Lett.* 43(20):1494–1497.

- [44] Vanderbilt D (1985) Optimally smooth norm-conserving pseudopotentials. *Phys. Rev. B* 32(12):8412–8415.
- [45] Bussi G, Donadio D, Parrinello M (2007) Canonical sampling through velocity rescaling. *J. Chem. Phys.* 126:014101.
- [46] Abraham MJ, et al. (2015) GROMACS: High performance molecular simulations through multi-level parallelism from laptops to supercomputers. *SoftwareX* 1-2:19–25.
- [47] Flyvbjerg H, Petersen HG (1989) Error estimates on averages of correlated data. *J. Chem. Phys.* 91(1):461–466.
- [48] Abramson EH, Bollengier O, Brown JM (2017) Water-carbon dioxide solid phase equilibria at pressures above 4 GPa. *Sci. Rep.* 7:821.
- [49] Dubrovinskaia N, Dubrovinsky L (2003) Whole-cell heater for the diamond anvil cell. *Rev. Sci. Instrum.* 74(7):3433–3437.
- [50] Abramson EH (2017) Three-phase melting curves in the binary system of carbon dioxide and water. *J. Phys.: Conf. Ser.* 950:042019.

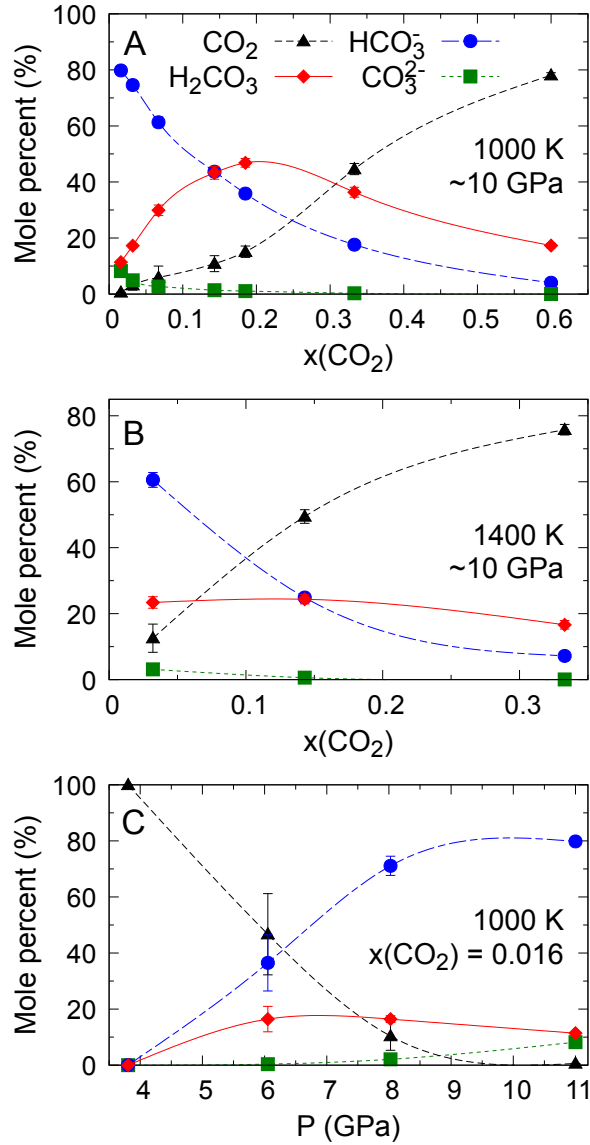


FIG. 1. Mole percents of CO<sub>2</sub>(aq), H<sub>2</sub>CO<sub>3</sub>(aq), HCO<sub>3</sub><sup>-</sup>, and CO<sub>3</sub><sup>2-</sup> in total dissolved carbon species in water. (A) The mole percents of carbon species as functions of the initial mole fraction of CO<sub>2</sub>(aq) ( $x(\text{CO}_2)$ ) at  $\sim 10$  GPa and 1000 K. (B) The mole percents of carbon species as functions of  $x(\text{CO}_2)$  at  $\sim 10$  GPa and 1400 K. (C) The mole percents of carbon species as functions of pressure at 1000 K and  $x(\text{CO}_2) = 0.016$ . Simulation data points are interpolated by cubic splines. Error bars are obtained by using the blocking method [47].

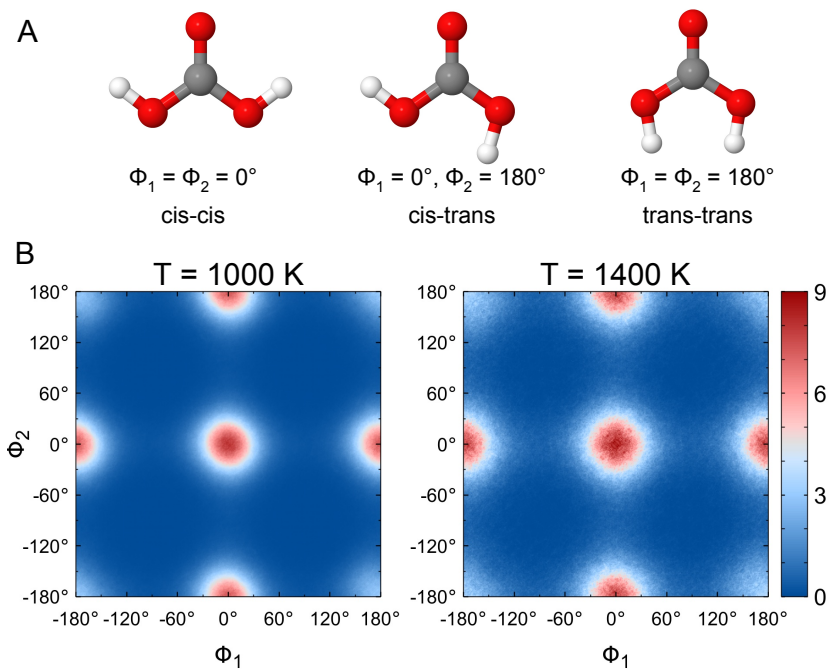


FIG. 2. Molecular geometry of  $\text{H}_2\text{CO}_3$  dissolved in water at  $\sim 10$  GPa, 1000 and 1400 K. (A) Three  $\text{H}_2\text{CO}_3$  conformers. The dihedral angles,  $\phi_1$  and  $\phi_2$ , are between the O=C and O-H bonds. (B) Probability densities of  $\phi_1$  and  $\phi_2$  (unit:  $10^{-5}/\text{degree}^2$ ).

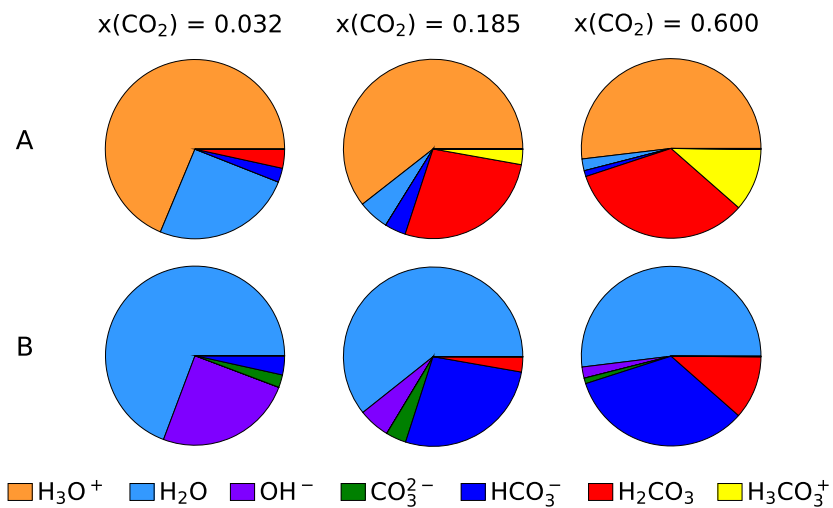


FIG. 3. Compositions of proton-donating and proton-accepting molecules or ions in  $\text{H}_2\text{CO}_3(\text{aq})$  formation and dissociation reactions, respectively, at  $\sim 10$  GPa and 1000 K. (A) Molecules or ions which donate protons to the reaction:  $\text{HCO}_3^- + \text{H}^+ \rightarrow \text{H}_2\text{CO}_3(\text{aq})$ . (B) Molecules or ions which accept protons from the backward reaction in (A).

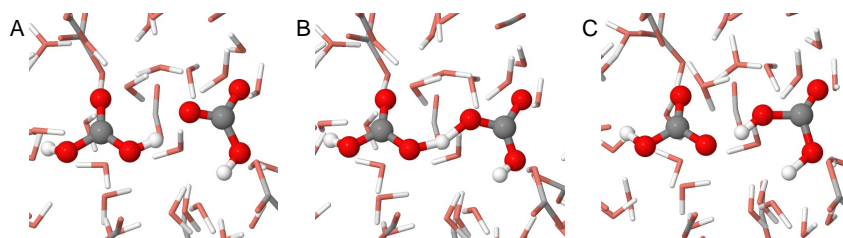


FIG. 4. Snapshots of the proton transfer from  $\text{H}_2\text{CO}_3(\text{aq})$  to  $\text{HCO}_3^-$ . (A) A cis-cis  $\text{H}_2\text{CO}_3$  molecule is approaching a  $\text{HCO}_3^-$  ion. (B) A proton is hopping from  $\text{H}_2\text{CO}_3(\text{aq})$  to  $\text{HCO}_3^-$ . (C)  $\text{HCO}_3^-$  and trans-trans  $\text{H}_2\text{CO}_3$  are formed after the reaction.

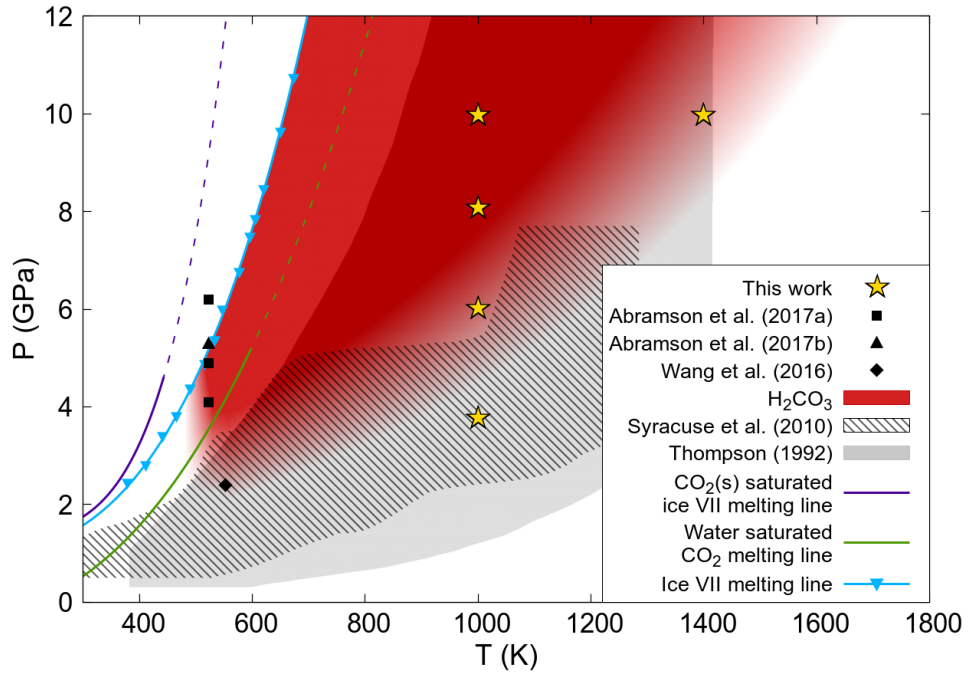


FIG. 5. Pressure-temperature range (in red) where  $\text{H}_2\text{CO}_3(\text{aq})$  is an important solute in water. The P-T conditions in the possible experimental observations of  $\text{H}_2\text{CO}_3$  are shown: Wang et al. [19], Abramson et al. (2017a) [20], and Abramson et al. (2017b) [48]. The grey shaded and hatched areas show the P-T conditions of water in Earth's upper mantle [32] and subducting slab surfaces (W1300 model) [33], respectively. The ice VII melting line is from Ref. [49]. The  $\text{CO}_2$ -saturated water and water-saturated  $\text{CO}_2$  melting lines are from Ref. [50]. Dashed lines are extrapolation.

## Supporting Information

Nore Stolte<sup>1</sup> and Ding Pan<sup>1,2,3,\*</sup>

<sup>1</sup>*Department of Physics, Hong Kong University  
of Science and Technology, Hong Kong, China*

<sup>2</sup>*Department of Chemistry, Hong Kong University  
of Science and Technology, Hong Kong, China*

<sup>3</sup>*HKUST Fok Ying Tung Research Institute, Guangzhou, China*

TABLE SI. AIMD simulation conditions. The pressures are calculated from simulations and models.  $x(\text{CO}_2)$  is the initial mole fraction of  $\text{CO}_2(\text{aq})$ , and  $n(\text{CO}_2)$  and  $m(\text{H}_2\text{O})$  are the numbers of  $\text{CO}_2$  and  $\text{H}_2\text{O}$  molecules, respectively, in the simulation box. Numbers in parentheses are standard deviations.

$x(\text{CO}_2)$	T (K)	$n(\text{CO}_2)$	$m(\text{H}_2\text{O})$	V ( $\text{cm}^3/\text{mol}$ )	$P^*$ (GPa)	$P^\circ$ (GPa)	$P^\dagger$ (GPa)	$P^\ddagger$ (GPa)
0.032	1000	2	60	11.59	10.26	12.32	10.5(0.2)	10.7(1.0)
0.067	1000	4	56	11.89	10.26	12.46	10.6(0.2)	10.3(1.1)
0.143	1000	8	48	12.59	10.26	12.49	10.7(0.2)	9.7(1.2)
0.185	1000	10	44	12.99	10.26	12.39	10.7(0.2)	9.4(1.2)
0.333	1000	16	32	14.48	10.26	11.71	10.6(0.2)	9.3(1.2)
0.600	1000	24	16	17.24	10.26	10.31	10.6(0.2)	10.0(1.2)
0.032	1400	2	60	12.20	10.26	12.23	10.3(0.2)	10.4(1.2)
0.143	1400	8	48	13.47	10.26	11.23	9.9(0.2)	9.2(1.3)
0.333	1400	16	32	15.67	10.26	9.88	9.4(0.2)	9.0(1.3)
0.016	1000	1	63	15.22	3.00	3.28	3.0(0.1)	3.8(0.8)
0.016	1000	1	63	13.50	5.00	5.65	5.0(0.2)	6.1(0.9)
0.016	1000	1	63	12.49	7.00	8.10	7.0(0.2)	8.0(1.0)

\* Duan and Zhang [1].

° Zhang and Duan [2].

† This work, force-field MD simulations.

‡ This work, AIMD simulations.



TABLE SII. Mole percents of carbon species in total dissolved carbon obtained from AIMD simulations (unit: %). Numbers in parentheses are standard deviations.

T (K)	P (GPa)	x(CO <sub>2</sub> )	CO <sub>2</sub>	CO <sub>3</sub> <sup>2-</sup>	HCO <sub>3</sub> <sup>-</sup>	H <sub>2</sub> CO <sub>3</sub>	H <sub>3</sub> CO <sub>3</sub> <sup>+</sup>	Pyrocarbonate
1000	10.7(1.0)	0.032	3.2(1.8)	4.9(0.4)	74.6(1.6)	17.3(0.8)	0.0(0.0)	0.0(0.0)
1000	10.3(1.1)	0.067	5.9(4.1)	2.7(0.1)	61.3(1.9)	29.9(1.9)	0.1(0.0)	0.0(0.0)
1000	9.7(1.2)	0.143	10.9(2.8)	1.4(0.1)	43.7(0.8)	43.3(2.3)	0.5(0.1)	0.3(0.1)
1000	9.4(1.2)	0.185	15.1(2.0)	1.1(0.0)	35.9(0.7)	46.8(1.5)	0.8(0.1)	0.3(0.1)
1000	9.3(1.2)	0.333	44.6(2.0)	0.3(0.0)	17.6(0.3)	36.4(1.8)	0.8(0.1)	0.3(0.1)
1000	10.0(1.2)	0.600	78.1(0.9)	0.0(0.0)	4.1(0.2)	17.3(0.8)	0.4(0.1)	0.1(0.0)
1400	10.4(1.2)	0.032	12.6(4.3)	3.1(0.3)	60.6(2.3)	23.4(1.8)	0.1(0.0)	0.3(0.3)
1400	9.2(1.3)	0.143	49.5(2.1)	0.6(0.0)	24.9(0.7)	24.4(1.4)	0.3(0.1)	0.4(0.2)
1400	9.0(1.3)	0.333	75.8(1.6)	0.0(0.0)	7.2(0.3)	16.6(1.3)	0.2(0.0)	0.1(0.0)
1000	3.8(0.8)	0.016	100.0(0.0)	0.0(0.0)	0.0(0.0)	0.0(0.0)	0.0(0.0)	0.0(0.0)
1000	6.1(0.9)	0.016	46.7(14.5)	0.4(0.1)	36.5(10.0)	16.4(4.5)	0.0(0.0)	0.0(0.0)
1000	8.0(1.0)	0.016	10.4(5.1)	2.1(0.2)	71.1(3.4)	16.4(1.2)	0.0(0.0)	0.0(0.0)

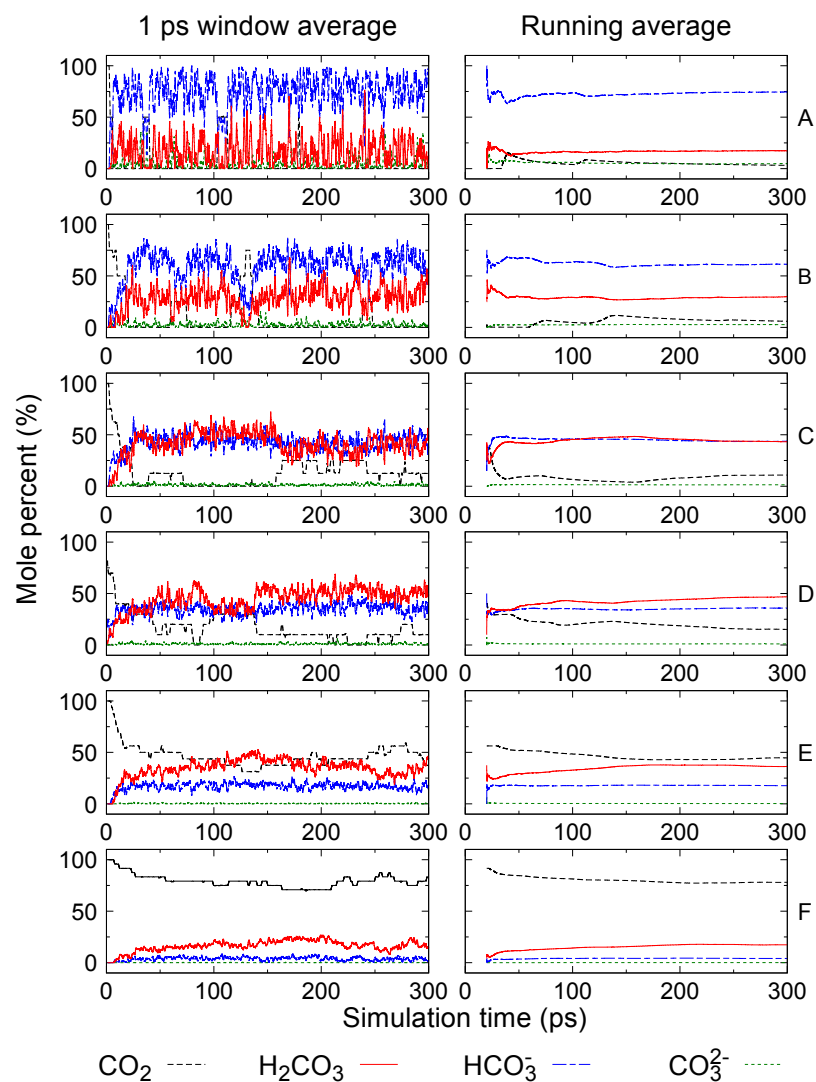


FIG. S1. Mole percents of carbon species as functions of simulation time in AIMD simulations. Left: 1-ps-window averages. Right: running averages. The initial mole fractions of  $\text{CO}_2(\text{aq})$  ( $x(\text{CO}_2)$ ) are (A) 0.032, (B) 0.067, (C) 0.143, (D) 0.185, (E) 0.333, and (F) 0.600. The temperature is 1000 K, and the pressure is  $\sim 10$  GPa.

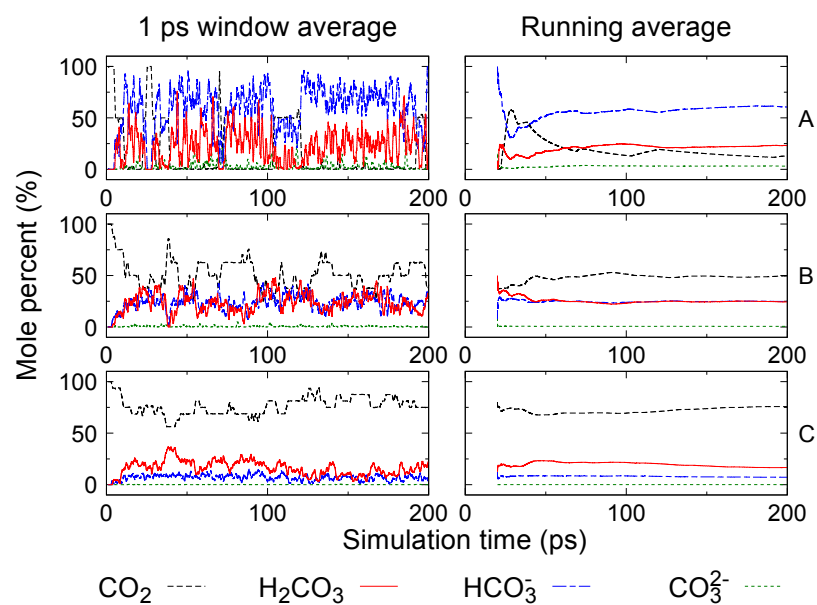


FIG. S2. Mole percents of carbon species as functions of simulation time in AIMD simulations. Left: 1-ps-window averages. Right: running averages. The initial mole fractions of  $\text{CO}_2(\text{aq})$  ( $x(\text{CO}_2)$ ) are (A) 0.032, (B) 0.143, and (C) 0.333. The temperature is 1400 K, and the pressure is  $\sim 10$  GPa.

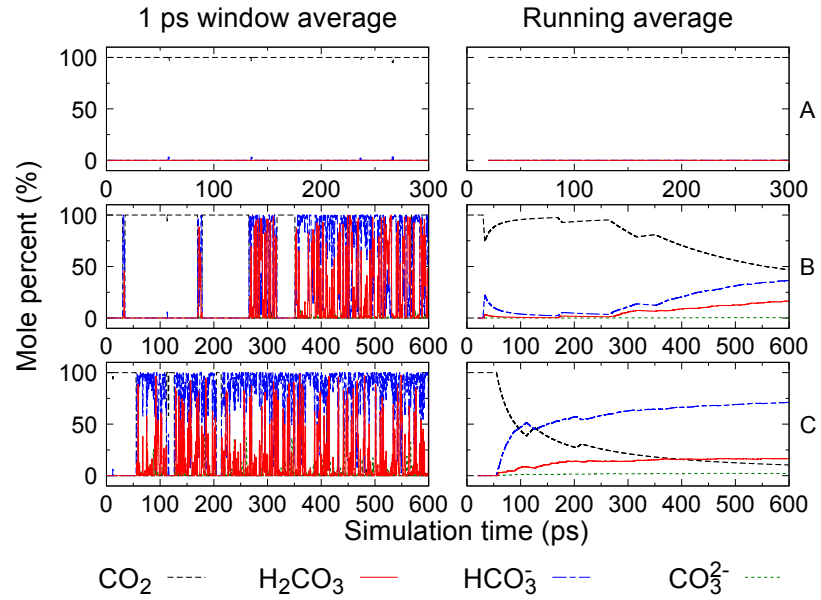


FIG. S3. Mole percents of carbon species as functions of simulation time in AIMD simulations. Left: 1-ps-window averages. Right: running averages. The pressures are (A) 3.8 GPa, (B) 6.1 GPa, and (C) 8.0 GPa. The temperature is 1000 K, and  $x(\text{CO}_2)$  is 0.016.

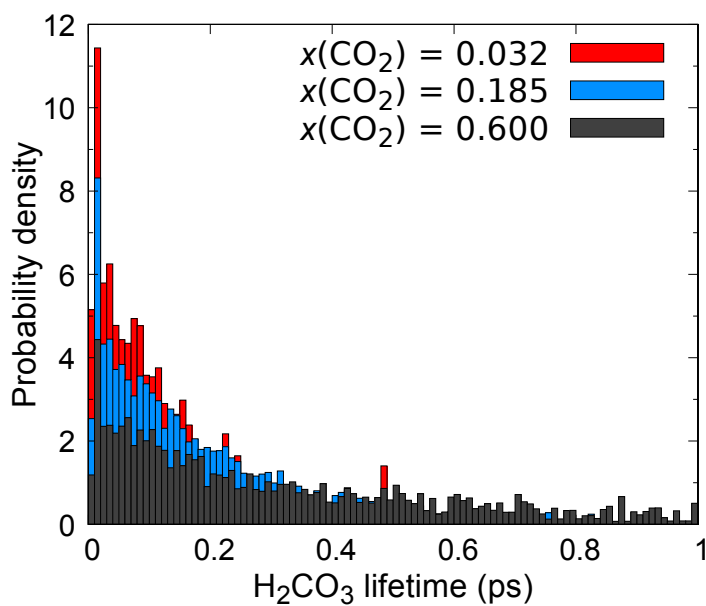


FIG. S4. Probability densities of lifetimes of  $\text{H}_2\text{CO}_3$  at  $\sim 10$  GPa and 1000 K. The initial mole fractions of  $\text{CO}_2(\text{aq})$  ( $x(\text{CO}_2)$ ) are 0.032, 0.185, and 0.600.

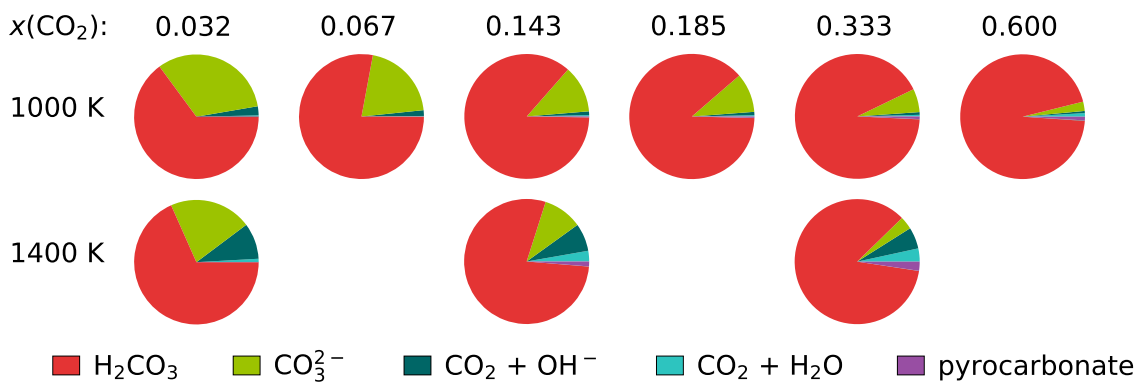


FIG. S5. Compositions of reaction products of  $\text{HCO}_3^-$  at  $\sim 10$  GPa. The reactions may be the decomposition ( $\text{HCO}_3^- \rightarrow \text{CO}_2 + \text{OH}^-$ ), the protonation ( $\text{HCO}_3^- + \text{H}^+ \rightarrow \text{H}_2\text{O} + \text{CO}_2$ ,  $\text{HCO}_3^- + \text{H}^+ \rightarrow \text{H}_2\text{CO}_3$ ), the deprotonation, or the formation of C-O-C bonds.

---

\* dingpan@ust.hk

- [1] Duan Z, Zhang Z (2006) Equation of state of the H<sub>2</sub>O, CO<sub>2</sub>, and H<sub>2</sub>O-CO<sub>2</sub> systems up to 10 GPa and 2573.15 K: Molecular dynamics simulations with ab initio potential surface. *Geochim. Cosmochim. Acta* 70(9):2311–2324.
- [2] Zhang C, Duan Z (2009) A model for C-O-H fluid in the Earth's mantle. *Geochim. Cosmochim. Acta* 73(7):2089–2102.